sustainability

MDPI

Article

Analysis of the Failure Characteristics and Main Controlling Factors of Surrounding Rocks Using the Standard Specimen with a Pre-Existing Hole

Zheng Wu [1], Jun Li [1], Wen-Long Zhang [2,*] and Chen Li [3]

[1] School of Energy and Mining Engineering, China University of Mining and Technology (Beijing), Beijing 100083, China
[2] School of Civil Engineering and Architecture, Qingdao Huanghai University, Qingdao 266427, China
[3] CCTEG Wuhan Engineering Company, Wuhan 430064, China
* Correspondence: wenlong0523@163.com

Abstract: To analyze the relationship between the butterfly-shaped plastic zone and stress in the rock with a single hole, we investigated the influence law of four factors, namely, the shape of the hole, the loaded confining pressure value, the bidirectional stress ratio, and the hole location on the volume of the butterfly-shaped plastic zone of the standard specimen with a single hole based on the orthogonal test and numerical simulation. The results show that: (I) The bidirectional stress ratio has a significant effect on the size of the plastic zone of the rock with a single hole, while the shape of the hole has no effect. (II) The basic value of confining pressure can weaken the sensitivity of the bidirectional stress ratio required to generate the butterfly-shaped plastic zone, that is, when the confining pressure value increases, the bidirectional stress ratio required to generate the butterfly-shaped plastic zone decreases, but there is always a certain value for the infinite expansion of the plastic zone. (III) The plastic zone of the rock with a single hole has a butterfly-shaped invariance, which means that the failure form of the surrounding rock around the hole will eventually evolve into a butterfly-shaped plastic zone under the state of a non-uniform stress field that reaches a certain bidirectional stress ratio. The research results of this paper have guiding significance for the stability control of the surrounding rock in underground engineering under the non-uniform stress field environment.

Keywords: mining non-uniform stress field; roadway surrounding rock stability; bidirectional stress ratio; butterfly-shaped plastic zone; orthogonal analysis

check for updates

Citation: Wu, Z.; Li, J.; Zhang, W.-L.; Li, C. Analysis of the Failure Characteristics and Main Controlling Factors of Surrounding Rocks Using the Standard Specimen with a Pre-Existing Hole. *Sustainability* **2022**, *14*, 14379. https://doi.org/10.3390/su142114379

Academic Editors: Haiyan Wang, Jia Lin and Guojun Zhang

Received: 10 October 2022
Accepted: 28 October 2022
Published: 3 November 2022

1. Introduction

When the external stress on the rock is greater than its own strength limit, a plastic zone will inevitably occur, which leads to its deformation and destruction [1,2]. Being in a relatively high-stress environment can lead to the surrounding rock instability in underground engineering [3–6], which is especially obvious in the field of roadway engineering [7,8]. Studies have shown that there is a positive correlation between the size of the plastic zone and the deformation of the surrounding rock under the same working conditions in the same lithology [9,10]. Therefore, it is extremely important to understand the morphological and dimensional development of the surrounding rock plastic zone under different stress states for the study of the deformation and failure mechanism of underground engineering and surrounding rock control technology.

For a long time, academics have always believed that the shape of the plastic zone around a circular hole is circular or elliptical [11], which is suitable for tunnel engineering excavated under isobaric or low-pressure stress conditions but has been proven to be unsuitable in tunneling projects disturbed by high bias stresses [12,13]. Ma Nianjie [14] et al. proposed the "*" distribution of the surrounding rock plastic zone for the mining roadway. After that, the team obtained the implicit equation of the surrounding rock plastic zone boundary of the circular roadway under the non-isobaric stress condition based on elastic-plastic mechanics [9], and innovatively proposed and developed the butterfly-shaped plastic zone theory [15–18]. This theory has made reasonable explanations for the phenomena of mining roadway roof fall [19], roadway asymmetric large deformation [20], coal and gas outburst [21], rock burst [22], and so on. Although few scholars have conducted special physical tests for the butterfly-shaped plastic zone theory, the failure patterns of the surrounding rock around the hole obtained from the related uniaxial tests [23,24], dynamic impact tests [25] and triaxial compression tests [26,27] of the prefabricated rock specimens verify the reality of the butterfly-shaped plastic zone from another perspective. In the literature [28], the influence of the mechanical properties of fillings on the failure mechanical characteristics of rocks with an elliptical hole was studied. The uniaxial compression test was carried out on the slab sandstone specimens containing prefabricated holes and filled with different ratios of cement mortar. When the loading stress reached the peak stress σ_c in all three specimens, the maximum principal strain contour of the specimens could clearly see the butterfly shape pattern, the maximum principal strain contour of the specimens can be seen in Figure 1. In the literature [29], during specimen loading experiments on marble containing prefabricated holes and simulating the damage process of specimens under uniaxial and biaxial compression conditions using PFC2D, it was found that macroscopic failure modes of both circular and square hole specimens showed X-like shape shear failure under certain stress condition; the failure modes of specimens can be seen in Figure 2. Recently, some important investigations [30,31] were performed to study the crack-tip plastic/damage zones under bidirectional stress. However, the more macroscopic scale plastic zone in rock engineering is also worthy of further study.

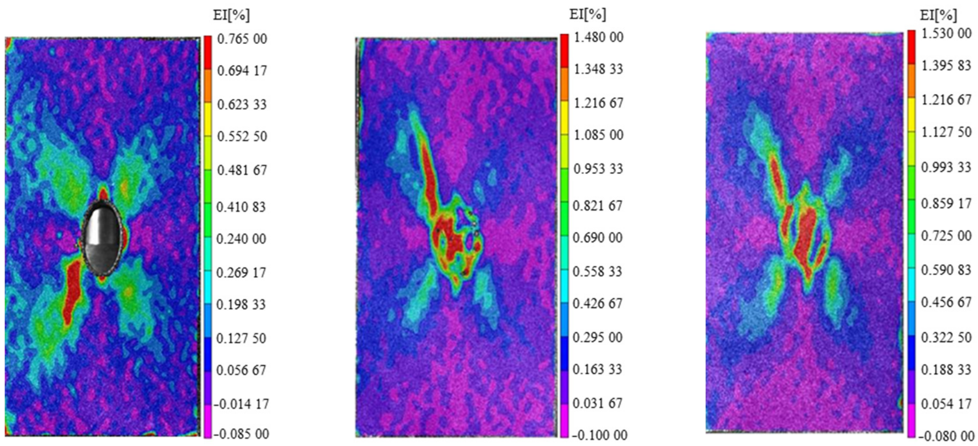

(**a**) (**b**) (**c**)

Figure 1. Maximum principal strain contour of specimens under different σ_c. (**a**) elliptical hole, (**b**) elliptical hole with type I filling material, (**c**) elliptical hole with type II filling material [28].

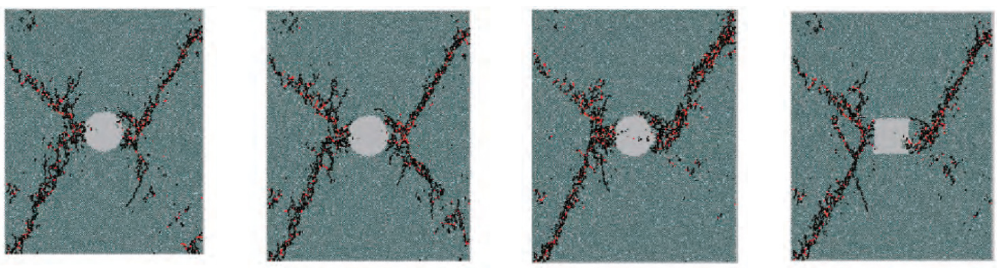

(**a**) $\sigma_3 = 5$ MPa (**b**) $\sigma_3 = 7.5$ MPa (**c**) $\sigma_3 = 10$ MPa (**d**) $\sigma_3 = 5$ MPa

Figure 2. Failure modes of specimens containing a single hole under biaxial compressions [29].

The butterfly-shaped plastic zone theory opens a precedent for the understanding of surrounding rock failure under a non-isobaric stress state in theory, but the previous studies mostly focus on the qualitative description of the formation of a butterfly plastic zone under a given condition. In this paper, orthogonal tests combined with numerical simulations will be used for quantitative analysis of the main controlling factors of the size of the butterfly-shaped plastic zone and the degree of influence of each factor on the volume of the butterfly-shaped plastic zone and study the characteristics of the butterfly-shaped plastic zone of the rock containing a single hole in a high bidirectional stress ratio environment. The results of this research can enrich the butterfly-shaped plastic zone theory and have certain theoretical and practical significance.

The main contributions are as follows:

(1) By using numerical simulation experiments based on the $L_{25}(5^6)$ orthogonal design, the influence of the shape of the hole, the loaded confining pressure value, the bidirectional stress ratio, and the hole location on the volume of the plastic zone in the standard specimen with a pre-existing hole were analyzed. Among these four factors, the bidirectional stress ratio has a significant effect, while the hole shape has no effect.

(2) Two characteristics of the butterfly-shaped plastic zone of rock containing a single hole are obtained. The first one is that the basic value of confining pressure can weaken the sensitivity of the bidirectional stress ratio required to generate the butterfly-shaped plastic zone. The other is that the plastic zone of the rock with a single hole has a butterfly-shaped invariance.

This paper is organized as follows: In Section 2, we described the butterfly-shaped plastic zone theory, the basic theory and formula of the orthogonal test, range analysis, and the analysis of variance. In Section 3, we demonstrate the design of the orthogonal test and the numerical simulation used in this paper. In Section 4, we present the results of numerical simulation experiments based on an orthogonal test design and perform a statistical analysis of the results. In Section 5, we further analyze the experimental results of the numerical simulations and obtain two characteristics of the butterfly-shaped plastic zone in rocks containing a hole, and give an engineering example to verify the characteristic, introduce similar results obtained by other researchers in their experiments as the experimental support for the numerical simulation results in this paper, and analyze the deficiencies and illustrate future work. Finally, the conclusions are provided in Section 6.

2. Methodology

2.1. Butterfly-Shaped Plastic Zone Theory

A large amount of measured data shows that the stress environment of underground engineering is non-uniform. Crustal stress is dominated by horizontal stress when shallower than 1000 m, and vertical stress is dominated at deeper than 1000 m, in China [32]. The bidirectional stress ratio of the regional stress field environment during mining can even reach 3~5 [11], which results in the roadway being in an extreme non-uniform stress field environment.

Assuming that the length of the deeply buried underground roadway is much larger than its diameter, the stress state does not change with the axial position of the roadway, and the surrounding rock of the roadway is a uniform continuous elastomer without creep and viscous behavior. Therefore, the plane strain method can be used to take any section as a representative in the infinite roadway length for research. The theoretical model is shown in Figure 3. In the figure, a is the radius of the roadway, r and θ are the polar coordinates of any point, P_1 is the maximum principal stress, and P_3 is the minimum principal stress, and define $\eta = P_1/P_3$.

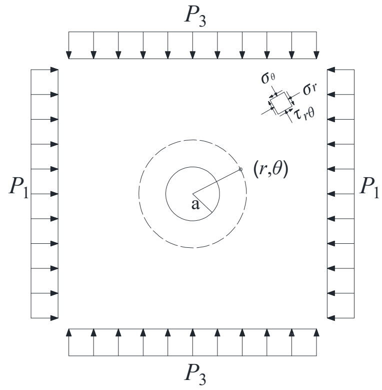

Figure 3. Mechanical model of circular roadway surrounding rock in a non-uniform stress field.

The roadway model is simplified to the hole problem of plane strain in elastoplastic mechanics. According to the theory of elasticity, when the medium satisfies the basic assumptions of homogeneity, continuity, and isotropy, the stress state of any point of the roadway surrounding rock can be expressed by Equation (1) [9].

$$\begin{cases} \sigma_r = \frac{P_3}{2}\left[(1+\eta)\left(1-\frac{a^2}{r^2}\right)+(\eta-1)\left(1-4\frac{a^2}{r^2}+3\frac{a^4}{r^4}\right)\cos 2\theta\right] \\ \sigma_\theta = \frac{P_3}{2}\left[(1+\eta)\left(1+\frac{a^2}{r^2}\right)-(\eta-1)\left(1+3\frac{a^4}{r^4}\right)\cos 2\theta\right] \\ \tau_{r\theta} = \frac{P_3}{2}\left[(1-\eta)\left(1+2\frac{a^2}{r^2}-3\frac{a^4}{r^4}\right)\sin 2\theta\right] \end{cases} \quad (1)$$

where σ_r, σ_θ, and $\tau_{r\theta}$ represent the radial stress, tangential stress, and shear stress at any point in the surrounding rock, respectively.

Using the Mohr–Coulomb criterion as the failure criterion of the rock at a certain point in the model, and taking Equation (1) into the Mohr–Coulomb criterion, the implicit equation of the plastic zone boundary of the circular roadway surrounding rock in the non-uniform stress field can be obtained [9]:

$$f\left(\frac{a}{r}\right) = K_1\left(\frac{a}{r}\right)^8 + K_2\left(\frac{a}{r}\right)^6 + K_3\left(\frac{a}{r}\right)^4 + K_4\left(\frac{a}{r}\right)^2 + K_5 = 0 \quad (2)$$

where:

$$K_1 = 9(1-\eta)^2$$

$$K_2 = -12(1-\eta)^2 + 6(1-\eta^2)\cos 2\theta$$

$$K_3 = 10(1-\eta)^2\cos^2 2\theta - 4(1-\eta)^2\sin^2\varphi\cos^2 2\theta - 2(1-\eta)^2\sin^2 2\theta - 4(1-\eta^2)\cos 2\theta + (1+\eta)^2$$

$$K_4 = -4(1-\eta)^2\cos 4\theta + 2(1-\eta^2)\cos 2\theta - 4(1-\eta^2)\sin^2\varphi\cos 2\theta - \frac{4C(1-\eta)\sin 2\varphi\cos 2\theta}{P_3}$$

$$K_5 = (1-\eta)^2 - \sin^2\varphi(1+\eta+\frac{2C\cos\varphi}{P_3\sin\varphi})^2$$

The calculation results for the given parameters (P_3 = 20 MPa, a = 2 m, C = 3 MPa, φ = 25°) for Equation (2) are shown in Figure 4. It can be seen that the shape and size of the plastic zone of the circular roadway surrounding rock change drastically with the change of the stress state of the surrounding rock: The plastic zone of the roadway is distributed in a circle when the bidirectional pressure is equal. With the increase of the bidirectional confining pressure ratio, the plastic zone shape develops from circular to ellipse and finally evolves into a butterfly shape, and the size of the plastic zone will expand rapidly after the butterfly-shaped plastic zone is created.

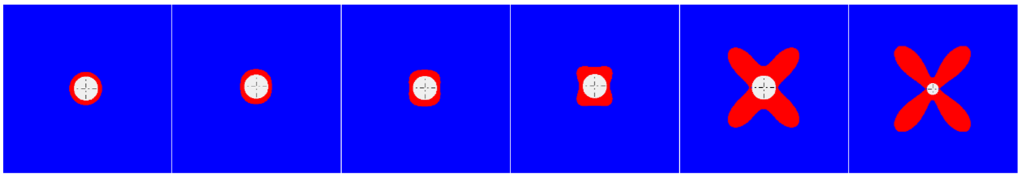

Figure 4. Evolution of the plastic zone under different stress states (The red part represents the plastic zone).

2.2. Orthogonal Test

The orthogonal test is an experimental design method to study multiple factors and multiple levels [33]. With the help of a standardized "orthogonal table", it selects experimental conditions scientifically, systematically and purposefully, arranges the experiments reasonably, and analyzes the experimental results scientifically using the principles of mathematical statistics. The orthogonal test selects some representative points from the full-scale test according to the orthogonality, and these representative points have the characteristics of being evenly distributed, comprehensive and comparable, which means that each level of each factor meets each level of the other factor once. The levels of each factor are comparable, and any level of each factor evenly includes the levels of other elements. When comparing different levels of a factor, the effects of other factors cancel each other out. Using orthogonal tests can achieve results equivalent to a large number of full-scale tests with a minimum number of tests.

The orthogonal test has the advantages of a small number of experiments, simple analysis method, good repeatability and high reliability, and can be used to figure out the influence of each factor on the experimental indexes and determine the priority of the factors through a small number of experiments with strong representation.

2.3. Range Analysis

The value of the range reflects the influence of the change of a selected factor on the dependent variable. The larger the range, the greater the difference between different levels of the factor, and the more significant the effect on the test results [33]. Therefore, the sensitivity analysis of the influencing factors was performed using the range analysis.

The range for factor i is calculated as:

$$R = \max k_i - \min k_i \tag{3}$$

$$k_i = \frac{1}{r} K_i \tag{4}$$

where i represents a certain level, K_i represents the sum of observations of a factor at the ith level, r represents the number of tests for a factor at a given level, k_i represents the mean value of the observations of a factor at the ith level.

2.4. Analysis of Variance

Range analysis cannot distinguish whether the difference in test results is caused by changes in the levels of the factors or by the random fluctuations of the test [34]. Therefore, using the analysis of variance (ANOVA) [35] was conducted to distinguish differences between test results caused by changes in factor levels from differences between test results caused by the random error fluctuation, and perform an F-test [36].

When the interaction of factors is not considered, the total sum of the square errors is S_T, the total degrees of freedom is d_T, the sum of the square errors of each factor is S_A, S_B, S_C, S_D, and the degrees of freedom are d_A, d_B, d_C, d_D, the sum of squares due to error is S_e, and the degree of freedom is d_e. The total sum of square errors of the factors can be decomposed as:

$$\begin{cases} S_T = S_A + S_B + S_C + S_D + S_e \\ S_i = \frac{1}{r}\sum_{j=1}^{m}\left(K_{ij}^2 - CT\right) \\ S_e = S_T - S_A - S_B - S_C - S_D \end{cases} \tag{5}$$

$$CT = \left(\sum_{i=1}^{n} k_i\right)^2 / n \tag{6}$$

$$\begin{cases} d_T = n - 1 \\ d_A = d_B = d_C = d_D = m - 1 \\ d_e = d_T - d_A - d_B - d_C - d_D \end{cases} \tag{7}$$

where i represents each factor (A, B, C, D), m represents the number of levels, r represents the number of replicate experiments performed at each level, K_{ij} represents the sum of all observations at the jth level of factor i, and k_i represents the observed value of the ith experiment of the orthogonal test.

3. Experiment Design

3.1. Orthogonal Test Design

To quantify the effect of different parameters, the method of the orthogonal test can comprehensively and scientifically conduct quantitative research on the plastic zone of the hole surrounding rock under non-isobaric stress conditions [37]. The influence of each factor on the volume of the plastic zone was investigated by conducting orthogonal tests with the results of triaxial compression simulation experiments on standard specimens with a prefabricated hole. The test has 4 factors: the shape of the hole, the value of the confining pressure, the bidirectional stress ratio η, and the offset distance between the center of the hole and the center of the specimen along the axis, each factor has 5 levels. The factors and levels are set as follows: 5 types of hole shapes are selected based on the actual engineering, which are (a) circle, (b) square, (c) rectangle with an aspect ratio of 3:5, (d) rectangle with an aspect ratio of 5:7, and (e) straight wall semi-circular arch, as shown in Figure 5. The test adopts the triaxial compression method to apply axial and confining pressure to the specimens, in which the stress ratio η of the axial pressure on the top surface and the confining pressure are 3.2, 3.4, 3.6, 3.8 and 4.0. The values of the confining pressures are 11 MPa, 12 MPa, 13 MPa, 14 MPa and 15 MPa. The offset distances are +1 cm, +0.5 cm, 0 cm, −0.5 cm, and −1 cm. The settings of each level of the orthogonal test are shown in Table 1.

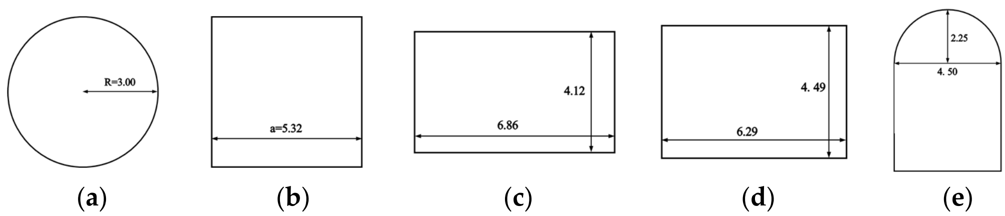

Figure 5. Different shapes of specimen holes: (**a**) Circle; (**b**) Square; (**c**) Rectangle with an aspect ratio of 3:5; (**d**) Rectangle with an aspect ratio of 5:7; (**e**) Straight wall semi-circular arch.

The rock mechanical parameters of the specimen are derived from the measured data of the siltstone in the Buertai mine in the Shendong mining area, China, as shown in Table 2. The size of the test specimen is a cylindrical standard specimen with a radius of 25 mm and a height of 100 mm. Considering the boundary problem during the test of specimens with a prefabricated hole, the circular hole with a radius of 3 mm is used as the reference, and the dimensions of other section forms are determined according to the principle of area equivalence. According to the determined factor levels, the $L_{25}(5^6)$ standard orthogonal table is selected for the orthogonal test, and the fifth column of this orthogonal table is selected as the blank column for random error analysis. Therefore, a total of 25 tests are required, all of which are numerical simulations.

Table 1. Factors and levels of numerical simulation orthogonal experiments.

Level	The Shape of the Hole	Confining Pressure (MPa)	Bidirectional Stress Ratio	Offset Distance (cm)
1	Circle	11	3.2	+1
2	Square	12	3.4	+0.5
3	Rectangle (3:5)	13	3.6	0
4	Rectangle (5:7)	14	3.8	−0.5
5	Straight wall semi-circular arch	15	4.0	−1

Table 2. Rock mechanics parameters.

Density (kg/m^3)	Young's Modulus	Poisson's Ratio	Cohesion (MPa)	Friction Angle (°)	Tensile Strength (MPa)
2456	9.1×10^9	0.19	5.2	35°	2.5

3.2. Numerical Simulation Design

FLAC^{3D} is an international analysis software for various types of geotechnical engineering. It has powerful calculation functions and extensive simulation capabilities, especially in the analysis of rock excavation failure problems [38–42]. The numerical simulation specimen models were created according to the specimen conditions determined in the orthogonal design described above, and the tetrahedral mesh was selected to divide the numerical simulation specimen models with a mesh size of 2 mm. Part of the model is shown in Figure 6. The bottom boundary of the specimen model was fixed in FLAC^{3D}, and the top and side surfaces of the specimen were compressed in the axial and circumferential surface according to the stress values designed in the orthogonal design, and the Mohr–Coulomb model is used in the calculation.

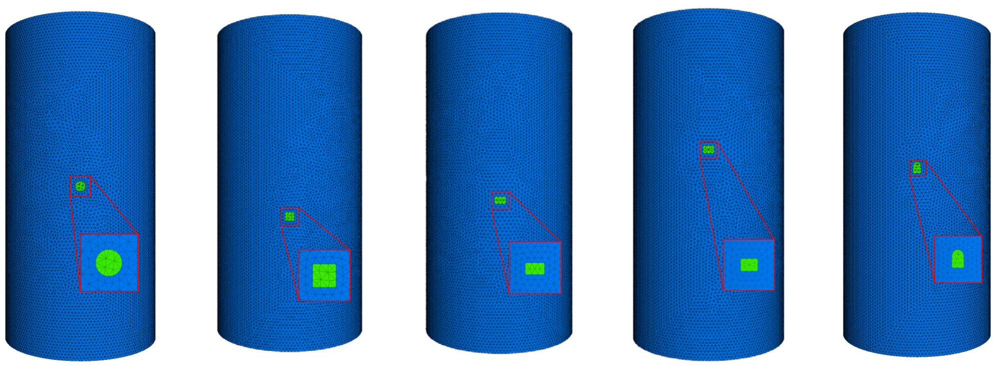

No. 3 No. 8 No. 15 No. 20 No. 24

Figure 6. Numerical simulation models.

4. Results Analysis

4.1. Test Results

After the numerical simulation models with different compression conditions are balanced, using the FISH language counts the plastic zone volume of the numerical model to obtain the failure volume of each specimen. Since the failure volume at the top and bottom boundaries of the model due to the end effect in the test is not caused by the hole, the plastic zone on both sides of the specimen model is removed when counting the plastic zone volume; only the butterfly-shaped failure volume of each specimen around the hole was recorded. The representative numerical calculation results are shown in Figure 7, and then we calculated the volume of the plastic zone in each set of experimental results and write the results of the calculated volume of the plastic zone in Table 3 as the result of the numerical simulation orthogonal test; the experiment setup and corresponding results can be seen in Figure 8. Figure 7 indicates the butterfly-shaped plastic zone. In reality, conjugate flaws may be generated for relatively brittle rocks. Thus, the subsequent failure behavior of rocks with conjugate cracks under engineering loads is also worthy of further study in the future, as the preliminary exploration presented by Feng et al. [43].

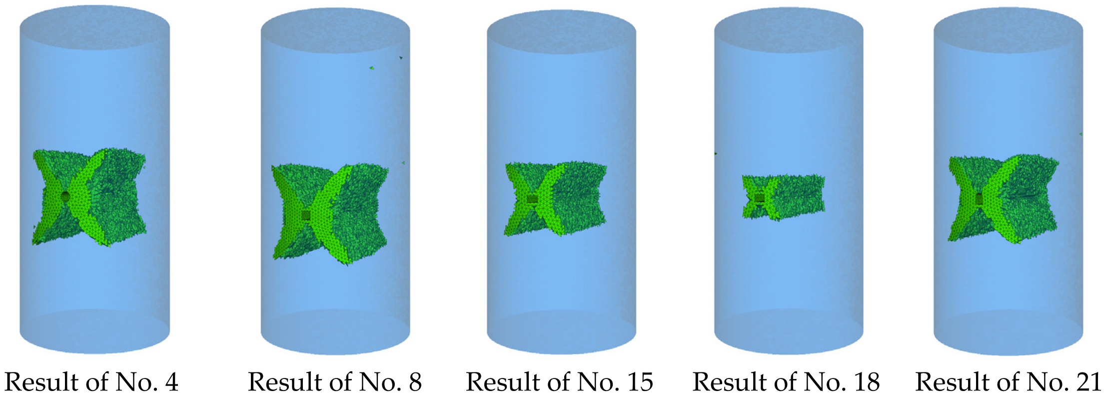

Figure 7. Part of the numerical simulation results.

Table 3. The result of the orthogonal experiment.

Experiment Number	Column					
	The Shape of the Hole	Confining Pressure (MPa)	Bidirectional Stress Ratio	Offset Distance (cm)	Blank	Volume of the Plastic Zone (cm^3)
1	Circle	11	3.2	+1	1	0.829105
2	Circle	12	3.4	+0.5	2	1.92394
3	Circle	13	3.6	0	3	3.91722
4	Circle	14	3.8	−0.5	4	11.1931
5	Circle	15	4.0	−1	5	60.5862
6	Square	11	3.4	0	4	2.38457
7	Square	12	3.6	−0.5	5	5.1885
8	Square	13	3.8	−1	1	11.7656
9	Square	14	4.0	+1	2	30.2792
10	Square	15	3.2	+0.5	3	3.21637
11	Rectangle (3:5)	11	3.6	−1	2	5.30551
12	Rectangle (3:5)	12	3.8	+1	3	8.87453
13	Rectangle (3:5)	13	4.0	+0.5	4	28.522
14	Rectangle (3:5)	14	3.2	0	5	3.86139
15	Rectangle (3:5)	15	3.4	−0.5	1	7.54838
16	Rectangle (5:7)	11	3.8	+0.5	5	6.80009
17	Rectangle (5:7)	12	4.0	0	1	17.8001
18	Rectangle (5:7)	13	3.2	−0.5	2	3.14766
19	Rectangle (5:7)	14	3.4	−1	3	6.04705
20	Rectangle (5:7)	15	3.6	+1	4	9.42452
21	Straight wall semi-circular arch	11	4.0	−0.5	3	9.40636
22	Straight wall semi-circular arch	12	3.2	−1	4	1.39334
23	Straight wall semi-circular arch	13	3.4	+1	5	2.49086
24	Straight wall semi-circular arch	14	3.6	+0.5	1	5.88783
25	Straight wall semi-circular arch	15	3.8	0	2	16.8152

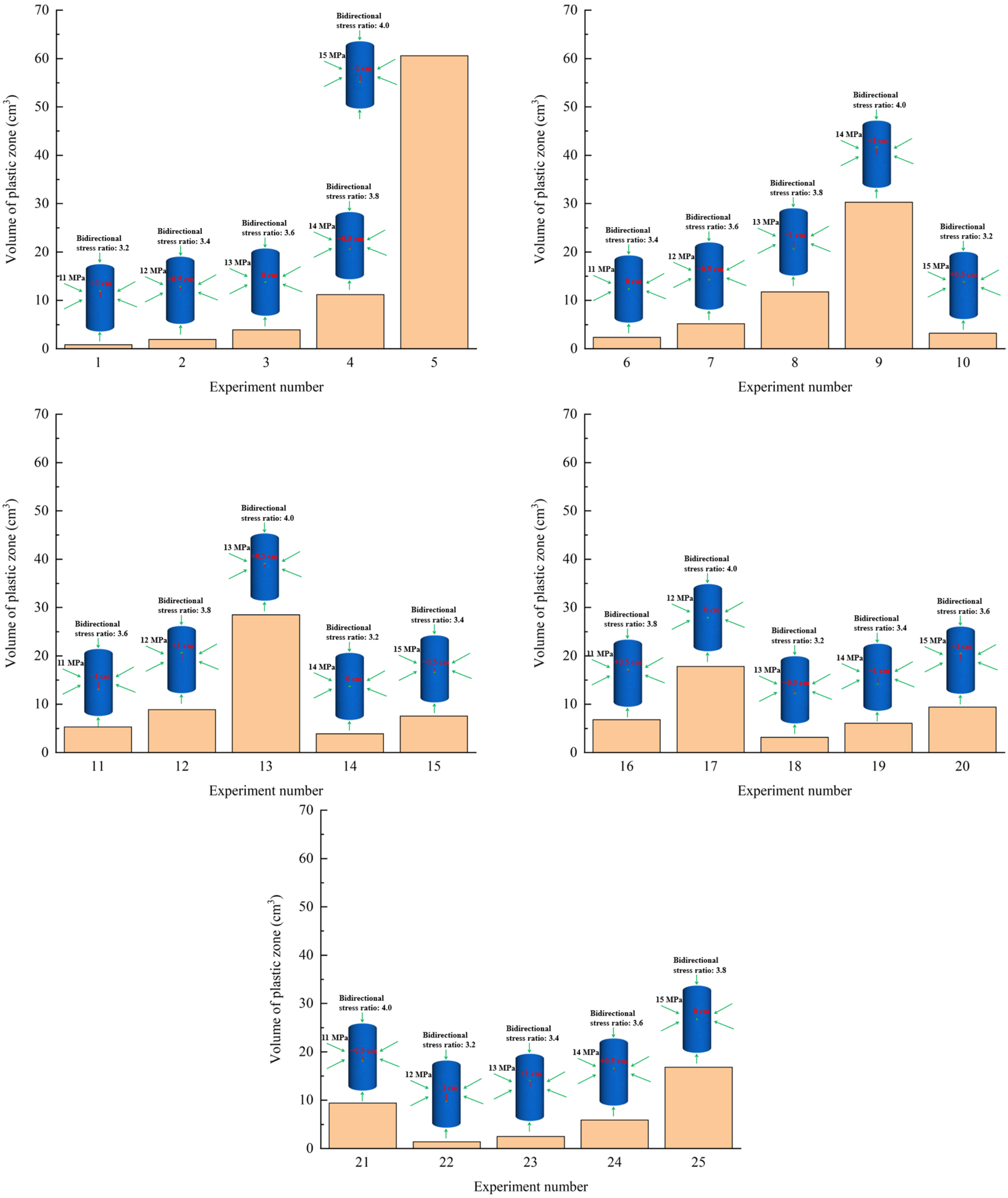

Figure 8. Experiment setup and corresponding results.

4.2. Range Analysis

The mean and range of the influence of different factors on the volume of the plastic zone in the orthogonal test are shown in Table 4. In addition, Table 4 also gives the blank column data which represents the experimental error. The results of the blank column are used to represent the experimental random error and determine the reliability of each factor and clarify whether it really affects the experiment results. Therefore, only when the range value of each factor is greater than the range value of the blank column can it indicate that the effect of this factor on the dependent variable exists.

Table 4. Results of the range analysis.

	Column					
	The Shape of the Hole	**Confining Pressure (MPa)**	**Bidirectional Stress Ratio**	**Offset Distance (cm)**	**Blank**	**Volume of the Plastic Zone (cm^3)**
K_1	78.449565	24.72564	12.44787	51.89822	43.83102	Total: 264.6086
K_2	52.83424	35.18041	20.3948	46.35023	57.47151	
K_3	54.11181	49.84334	29.72358	44.77848	31.46153	
K_4	43.21942	57.26857	55.44852	36.484	52.91753	
K_5	35.99359	97.59067	146.5939	85.0977	78.92704	
k_1	15.68991	4.945127	2.489573	10.37964	8.766203	Total average: 10.58435
k_2	10.56685	7.036082	4.07896	9.270046	11.4943	
k_3	10.82236	9.968668	5.944716	8.955696	6.292306	
k_4	8.643884	11.45371	11.0897	7.2968	10.58351	
k_5	7.198718	19.51813	29.31877	17.01954	15.78541	
R	8.491195	14.573007	26.829199	9.72274	9.493102	

From Table 4, it can be seen that the range values of each test factor are, in descending order, 26.829199, 14.573007, 9.72274, 9.493102, and 8.491195. Organizing the data in Tables 3 and 4 as shown in Figure 9: The C factor (Bidirectional stress ratio) has the largest range value, followed by the B factor (Confining pressure), then the D factor (Distance of hole offset from the center of the specimen) and the A factor (The shape of the hole), the sensitivity of the plastic zone volume to each factor is C–B–D–A. This indicates that for the volume of the butterfly-shaped plastic zone of the specimens, the C factor (Bidirectional stress ratio) plays the most significant role. In addition, the range of the A factor (the shape of the hole) is smaller than the range of the blank column, so it can be concluded that the shape of the hole is not significant for the size of the butterfly-shaped plastic zone volume of the specimens.

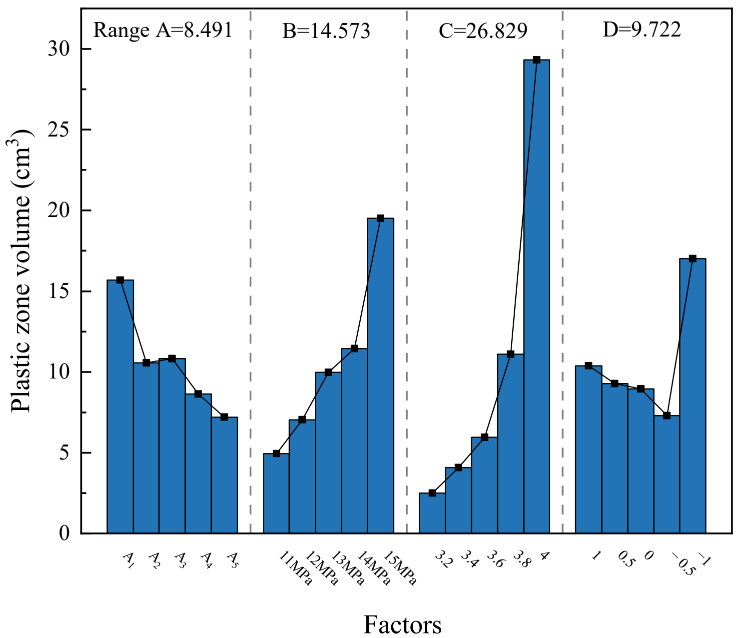

Figure 9. Results of range analysis (A1: Circle, A2: Square, A3: Rectangle (3:5), A4: Rectangle (3:5), A5: Straight wall semi-circular arch).

4.3. Analysis of Variance

In this experiment, a blank column was arranged in the orthogonal table for error estimates. The ANOVA was performed on the results of this orthogonal test, and the calculation results are shown in Table 5.

Table 5. Results of ANOVA.

	Sum of the Square	Degree of Freedom	Mean Square	F	Significance
The shape of the hole	206.758	4	51.690	0.830	0.542
Confining pressure (MPa)	626.692	4	156.673	2.516	0.124
Bidirectional stress ratio	2403.028	4	600.757	9.646	0.004
Offset distance (cm)	283.207	4	70.802	1.137	0.405
Error	498.245	8	62.281		

It can be seen from the ANOVA results in Table 5 that the significance of factor C (Bidirectional stress ratio) is less than 0.05, which indicates that the bidirectional stress ratio has a significant effect on the size of the butterfly-shaped plastic zone of the specimens, and the significance values of all other factors are greater than 0.05, which indicates that none of the other factors are significant.

5. Discussion

In addition to the statistical analysis results obtained by the range analysis and variance analysis of the experimental results, some potential characteristics of the butterfly-shaped plastic zone can be seen from the previous experimental results. This section will discuss and analyze the properties of the butterfly plastic zone that may exist in the above section.

(1) The basic value of confining pressure can weaken the sensitivity of the bidirectional stress ratio required to generate the butterfly-shaped plastic zone

For the 1st, 6th, 11th, 16th, and 21st test results in the orthogonal test, it can be found that under the same confining pressure value, with the increase of the bidirectional stress ratio, the volume of the butterfly plastic zone generated gradually increases, indicating that with the increase of confining pressure, the bidirectional stress ratio required for the emergence of butterfly-shaped plastic zone is decreasing.

To verify this characteristic, only the effect of bidirectional stress ratio changes on the volume of the plastic zone is studied by the control variable method. The hole shape of the model is circular, the radius is 2.5 m, the rock cohesion C is 3 MPa and the internal friction angle $\varphi = 30°$, using numerical simulation to obtain the size of the plastic zone under different confining pressure values and bidirectional stress ratios. The maximum damage depth of the surrounding rock under different conditions is shown in Figure 10a. The shapes and sizes of the plastic zone when the bidirectional stress ratio is 2.8 are shown in Figure 10b.

It can be seen from Figure 10 that the pattern of the plastic zone curve under different confining pressure values is basically the same; all of them have limited changes in the size of the plastic zone with the increase of the bidirectional stress ratio before the butterfly-shaped plastic zone formation, and the increase of the bidirectional stress ratio will lead to the sudden increase in the size of the plastic zone after butterfly-shaped plastic zone formation, and all of them have the ultimate bidirectional stress ratio value of infinite expansion of the plastic zone. However, the difference is mainly manifested in the different accelerated destabilization inflection points and ultimate values of infinite expansion of the plastic zone under different values of confining pressure, that is, the larger the confining pressure value, the smaller the inflection point and ultimate value, the stronger the sensitivity of the surrounding rock plastic zone size to the confining pressure ratio. For example, the maximum dimensions of the plastic zone for the same $\eta = 2.8$ are 1.1 m, 4.4 m, and 5.9 m under the confining pressure values of 5 MPa, 15 MPa, and 25 MPa, respectively, with huge differences. Define the bidirectional stress ratio where the damage of the butterfly plastic zone tends to infinity as the ultimate bidirectional stress ratio (UBSR), and the bidirectional stress ratio when the plastic zone shape changes from a circle or ellipse to a butterfly shape as the trigger bidirectional stress ratio (TBSR). The values are shown in Table 6.

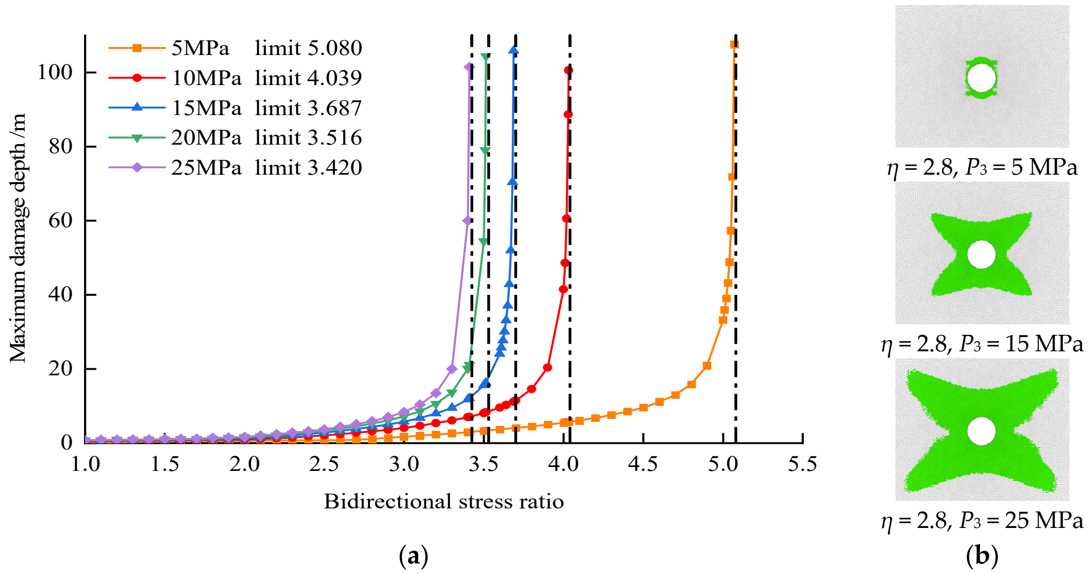

Figure 10. The plastic zone under different confining pressure and bidirectional stress ratios. (**a**) The response curve of the maximum damage depth in the plastic zone to the confining pressure and bidirectional stress ratio; (**b**) Plastic zone morphology and dimensions.

Table 6. TBSR and UBSR under different confining pressures.

	5 MPa	10 MPa	15 MPa	20 MPa	25 MPa
TBSR	2.9	2.3	2.2	2.1	2.0
UBSR	5.08	4.039	3.687	3.516	3.42

In summary, the minimum bidirectional stress ratio required for butterfly failure to occur in the rock containing a hole decrease with the increase of the stress base, which means, under the high confining pressure condition, even a small change in the bidirectional stress ratio can lead to a sharp expansion of the maximum damage depth in the plastic zone, or even a malignant infinite expansion. This also indicates that the confining pressure value of the roadway increases with the increase of the mining depth, and the bidirectional stress ratio required for butterfly failure of the roadway surrounding rock is continuously decreasing, which is consistent with the fact that the roadway is more prone to severe deformation damage and even dynamic disasters in actual deep mining situation.

(2) Butterfly shape invariance of plastic zone

According to the results obtained from the numerical simulation conducted in the previous section, when the rock specimen with a single hole is under a certain stress condition and reaches the triggering stress range of the butterfly plastic zone, the plastic zone morphology will always be butterfly-shaped regardless of whether the hole location is located in the center of the specimen, whether the specimen is a standard cylindrical specimen, and whether the hole shape is circular, as shown in Figure 11. Only when the stress base and the bidirectional stress ratio change, the shape of the hole plastic zone changes from a circle to an ellipse to a butterfly, or the size of the butterfly-shaped plastic zone changes with the stress state.

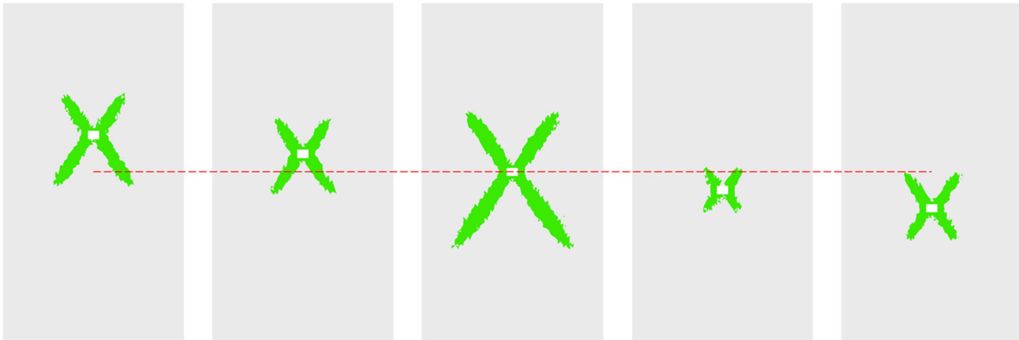

(a)

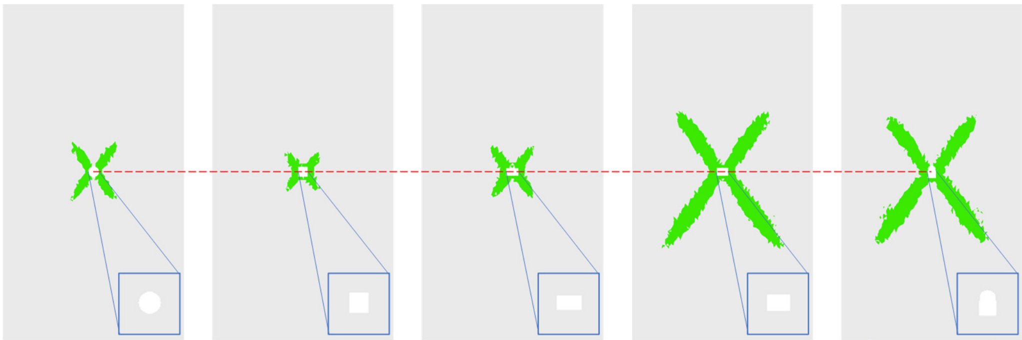

(b)

Figure 11. Longitudinal section of specimens. (**a**) Different locations of the hole. (**b**) Different shapes of the hole.

Based on the above analysis, it can be considered that when the stress around the hole reaches a certain stress base and non-uniform state, the plastic zone has the characteristic of butterfly shape invariance, that is, the final plastic zone of the hole will show a butterfly shape, and the shape does not change with the change of hole location and hole shape.

(3) Engineering example analysis

In the previous study, the article [44] investigated the non-uniform deformation damage in the 31115 ventilation roadway of the Lijiahao coal mine caused by the influence of advance abutment pressure at the working face. The Lijiahao coal mine is located in Dongsheng District, Ordos City, Inner Mongolia Autonomous Region, China as shown in Figure 12, and its 31115 working face has an average burial depth of 250 m and an average coal seam thickness of 6 m. Note that the 31115 working face rock stratum structure and working face layout are shown in Figure 13. The direct roof of the 31115 working face is mainly siltstone and fine-grained sandstone. The main roof is sandy mudstone with an average thickness of 9 m. The direct floor is sandy mudstone and siltstone. The strike length of the 31115 working face is 2600 m, and the dip length is 300 m. The north of the 31115 working face is the goaf of the 31114 working face, and the south side is the 31116 working face prepared to be arranged. The 31115 working face adopts a double lane arrangement, the 31115 working face ventilation roadway was a 31114 working face auxiliary transportation lane before, the roadway section size is 5.2 m × 3.56 m, used for retrieving air. The coal pillar width between the main and auxiliary transport roadway is 20 m.

Using FLAC^{3D}, we numerically simulated the stress and plastic zone of 31115 ventilation roadway. When the 31115 working face is mined for 300 m, collect the maximum and minimum principal stresses and the angle between the maximum principal stress and the vertical direction at 5 m and 10 m in front of the 31115 working face. The angle between the maximum principal stress and the vertical direction is specified as positive in the counterclockwise direction; the data are shown in Table 7, the plastic zone of the roadway surrounding rock at the corresponding location, as shown in Figure 14.

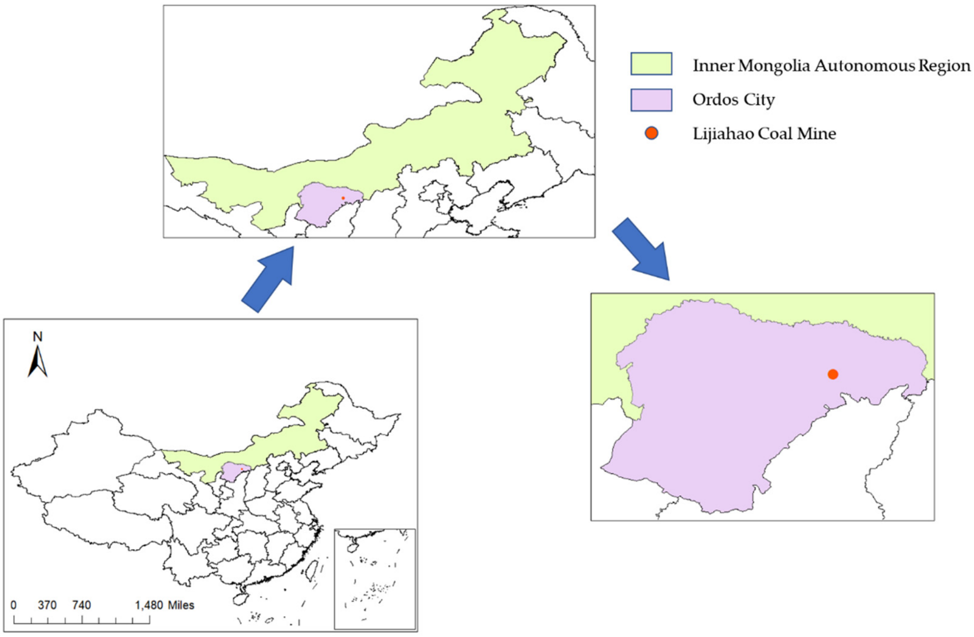

Figure 12. Location of the Lijiahao Mine.

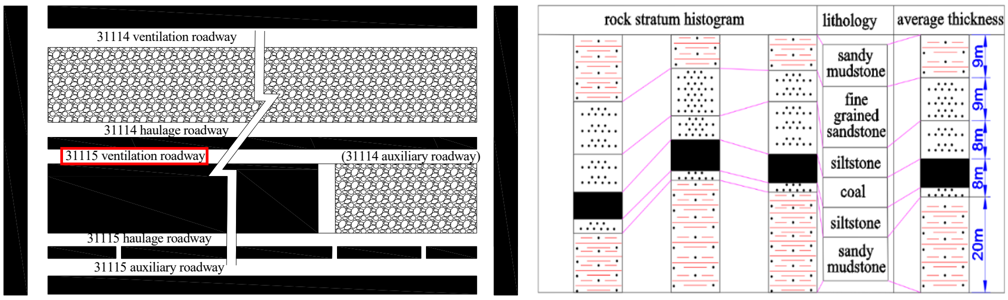

Figure 13. Working face layout and rock stratum structure.

Table 7. Principal stress information of the 31115 ventilation roadway.

The Distance Ahead of the Working Face	Max Principal Stress	Min Principal Stress	The Ratio of Max and Min Principal Stress	The Angle of the Max Principal Stress
5 m	12.71	4.62	2.75	15°
10 m	11.73	5.10	2.30	−51°

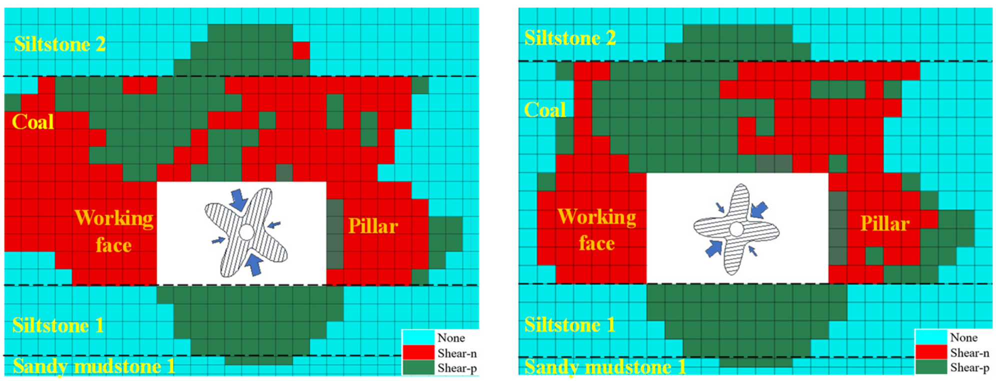

(**a**) (**b**)

Figure 14. Plastic zone distribution around the 31115 ventilation roadway. (**a**) 5 m in front of the 31115 working face. (**b**) 10 m in front of the 31115 working face.

From the simulation results, it can be seen that under the influence of advance abutment pressure in front of the working face, the principal stress direction of the roadway surrounding rock is deflected by the influence of the working face mining, and the maximum principal stress is deflected towards the present mining working face. The bidirectional stress ratio is 2.75 at the position of 5 m ahead of the working face and 2.30 at the position of 10 m ahead of the working face, both of which have the stress ratio requirements for the formation of a butterfly plastic zone, under the influence of high bidirectional stress ratio, the roadway surrounding rock also shows an irregular butterfly-like plastic zone form. Affected by the direction of the maximum and minimum principal stresses in the regional stress field, the maximum damage depth area in the surrounding rock plastic zone, the butterfly leaf area, is also deflected. As mentioned earlier, the butterfly leaf usually appears near the angular parallels of the maximum and minimum principal stresses. The angle between the maximum and minimum principal stress angle parallels and the vertical direction is 30° and 6°, respectively, at 5 m and 10 m ahead of the working face in the 31115 ventilation roadway. The largest damaged area of the surrounding rock plastic zone, or the butterfly leaf, is located near the roadway roof and the two sides. In addition, the coal seam is thick, and the direct roof of the roadway is coal, resulting in a large range of plastic zones on the roadway roof and the two sides. The depth of the plastic zone of the roadway roof is 4.5 m; in this case, it is difficult to effectively guarantee the safety and stability of the roadway by simply using ordinary anchor support.

This simulation example verifies the butterfly invariance mentioned above, that is, when the bidirectional stress ratio exceeds a certain value, the plastic zone of the hole will show a butterfly shape, and the maximum damage depth area in the surrounding rock plastic zone, or the butterfly leaf area, appears near the angle parallels of the maximum and minimum principal stresses.

(4) Similar results from laboratory experiments by other researchers

At present, the butterfly-shaped plastic zone theory proposed by our research group is becoming mature, which explains the theoretical occurrence mechanism of practical engineering problems such as mining roadway roof fall [19], roadway asymmetric large deformation [20], coal and gas outburst [21], rock burst [22]. Although no specific theoretical tests have been conducted, the conclusions obtained from laboratory tests by related scholars can indirectly prove the reliability of the theory and the numerical simulation results in this paper.

Eyvind Aker et al. [23] performed triaxial compression tests on sandstone specimens with prefabricated holes, the macroscopic crack expansion morphology and acoustic emission source distribution statistics of the specimens were similar to the butterfly shape. The experimental results are shown in Figure 15.

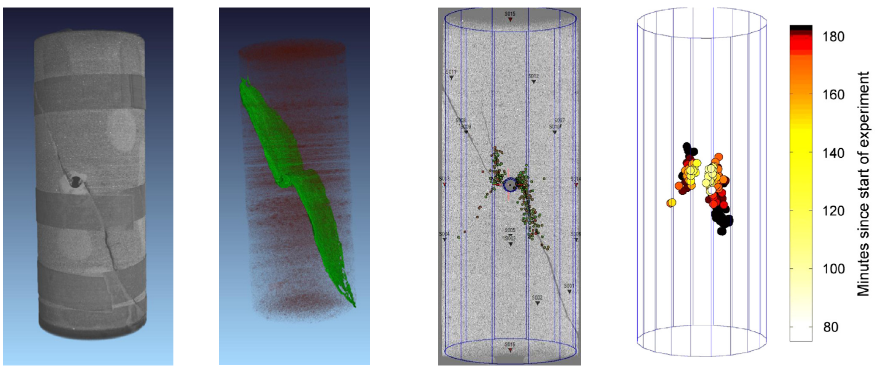

(**a**) (**b**) (**c**) (**d**)

Figure 15. CT scan and locations of events. (**a**) Surface of the whole sample. (**b**) 3D high-resolution X-ray CT scan of the sample after testing Pore volume (red), fractured volume (green), (**c**) Locations of 305 events overlaid on a 2D longitudinal cross-sectional cut of the 3D X-ray CT image, (**d**) 162 events selected for moment tensor inversion, colored according to origin time in minutes after the start of the experiment [23].

According to the literature [25], the impact compression test was carried out on the yellow sandstone specimen with a certain angle between the bedding plane and the loading direction on a separate Hopkinson compression bar test platform with a bar diameter of 75 mm, and the specimens with inclination angles of 60° to 90° eventually develop an X-like shape shear failure through the bedding. Some of the results are shown in Figure 16.

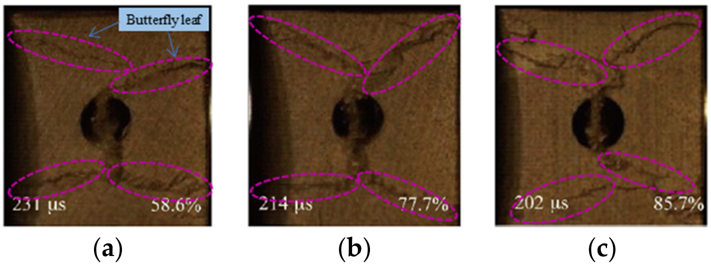

Figure 16. Crack in highly dipping specimens (**a**) $\varphi = 60°$, (**b**) $\varphi = 75°$, (**c**) $\varphi = 90°$ [25].

In literature [28,29] introduced in the Introduction section, the maximum principal strain contour of the specimens and the damage pattern simulated using PFC both have a clear butterfly shape. The results of the loading experiments on the specimens with a hole in the laboratory tests mentioned above all show the form of a butterfly plastic zone. Although the studies above did not mention the butterfly plastic zone, they all play a role in arguing that the butterfly damage will occur under certain bidirectional stress ratio loading conditions in the rock specimens containing a hole and can indirectly prove the reliability of the numerical simulation results in this paper.

(5) Deficiencies and Prospects

The butterfly-shaped plastic zone theory can well explain the phenomenon of non-uniform deformation of roadway, mining roadway roof fall, and rock burst disasters, but it is still impossible to accurately detect the boundary of the plastic zone where butterfly failure occurs in the engineering field. In addition, there are still some discrepancies between the complex working conditions at the engineering site and the theoretical analysis under ideal conditions. In the future, the theory should be enriched with three-dimensional large-scale laboratory experiments and should pay more attention to the refined detection of the plastic failure boundary of the surrounding rock at the engineering site, so that the theory can be better integrated with the practice and better guide the engineering applications.

6. Conclusions

(1) The bidirectional stress ratio has a significant effect on the volume of the butterfly-shaped plastic zone in the surrounding rock around the hole, followed by the confining pressure value, while the shape of the hole has no effect on the volume of the butterfly-shaped plastic zone in the specimen.

(2) The basic value of confining pressure can weaken the sensitivity of the bidirectional stress ratio required to generate the butterfly-shaped plastic zone. As the confining pressure value increases, the bidirectional stress ratio required for the occurrence of the butterfly-shaped plastic zone decreases. After the occurrence of the butterfly plastic zone, with the increase of the basic value of confining pressure, the bidirectional stress ratio required for the abrupt increase in the volume of the butterfly-shaped plastic zone and the infinite expansion of the plastic zone both decrease.

(3) The failure form of the surrounding rock around the hole has butterfly invariance under the state of non-uniform stress field that reaches a certain bidirectional stress ratio, that is, when the basic value of the confining pressure and bidirectional stress ratio reaches the threshold value, the shape of the plastic zone of the hole surrounding rock under this stress environment is not affected by the location and shape of the hole and will eventually evolve into a butterfly shape.

Author Contributions: Conceptualization, Z.W. and C.L.; methodology, Z.W.; software, Z.W.; validation, C.L., W.-L.Z. and J.L.; formal analysis, Z.W. and C.L.; investigation, J.L.; data curation, J.L.; writing—original draft preparation, Z.W.; writing—review and editing, C.L. and W.-L.Z. All authors have read and agreed to the published version of the manuscript.

Funding: This research was funded by the National Natural Science Foundation of China, grant number 52004289, and the China Postdoctoral Science Foundation, general program, grant number 2021M700427.

Institutional Review Board Statement: Not applicable.

Informed Consent Statement: Not applicable.

Data Availability Statement: The data presented in this study are available on request from the corresponding author.

Conflicts of Interest: The authors declare no conflict of interest.

References

1. Cai, M. *Rock Mechanics and Engineering*; China Science Publishing & Media Ltd.: Beijing, China, 2013.
2. Kang, H. Spatial Scale Analysis on Coal Mining and Strata Control Technologies. *J. Min. Strat. Control Eng.* **2020**, *2*, 5–30.
3. Cai, M. Key theories and technonogies for surrounding rock stability and ground control in deep mining. *J. Min. Strat. Control Eng.* **2020**, *2*, 033037.
4. Wang, X.; Meng, F.-B. Statistical analysis of large accidents in China's coal mines in 2016. *Nat. Hazards* **2018**, *92*, 311–325. [CrossRef]
5. Zhang, G.; Li, Q.; Zhang, Y.; Du, F. Failure characteristics of roof in working face end based on stress evolution of goaf. *Géoméch. Geophys. Geo-Energy Geo-Resour.* **2021**, *7*, 53. [CrossRef]
6. Du, F.; Wang, K.; Zhang, X.; Xin, C.; Shu, L.; Wang, G. Experimental Study of Coal–Gas Outburst: Insights from Coal–Rock Structure, Gas Pressure and Adsorptivity. *Nonrenewable Resour.* **2020**, *29*, 2481–2493. [CrossRef]
7. Andrews, P.; Butcher, R.; Ekkerd, J. The geotechnical evolution of deep-level mechanized destress mining at South Deep mine. *J. S. Afr. Inst. Min. Met.* **2020**, *120*, 33–40. [CrossRef]
8. Duan, C.; Zheng, Q.; Xue, J.; Yu, G.; Luo, Y. Experimental study on zonal failure discontinuous deformation of deep surrounding rock under different working conditions. *J. Min. Strat. Control Eng.* **2021**, *3*, 9.
9. Zhao, Z.Q. *Mechanism of Surrounding Rock Deformation and Failure and Control Method Research in Large Deformation Mining Roadway*; China University of Mining and Technology (Beijing): Beijing, China, 2014.
10. Li, C.; Wu, Z.; Zhang, W. A case study on asymmetric deformation mechanism of the reserved roadway under mining influences and its control techniques. *Geomech. Eng.* **2020**, *22*, 449–460.
11. Qian, M.; Shi, P.; Xu, J. *Mining Pressure and Strata Control*; China University of Mining and Technology Press: Xuzhou, China, 2010; pp. 98–101.
12. Wang, W.; Dong, E.; Yuan, C. Boundary equation of plastic zone of circular roadway in non-axisymmetric stress and its application. *J. China Coal Soc.* **2019**, *44*, 105–114.
13. Wu, X.; Wang, J.; Wang, W.; Tian, C.; Bu, Q.; Wu, L. Study on the Stage Failure Mechanism and Stability Control of Surrounding Rock of Repeated Mining Roadway. *Adv. Civ. Eng.* **2020**, *2020*, 8866559. [CrossRef]
14. Ma, N.; Hou, C. *Theory and Application of Mining Pressure in Mining Roadway*; China Coal Industry Publishing House: Beijing, China, 1992.
15. Ma, N.; Li, J.; Zhao, Z. Distribution of the deviatoric stress field and plastic zone in circular roadway surrounding rock. *J. China Univ. Min. Technol.* **2015**, *44*, 206–213.
16. Ma, N.; Zhao, X.; Zhao, Z.; Li, J.; Guo, X. Stability analysis and control technology of mine roadway roof in deep mining. *J. China Coal Soc.* **2015**, *40*, 2287–2295.
17. Zhao, Z.; Ma, N.; Liu, H.; Guo, X. A butterfly failure theory of rock mass around roadway and its application prospect. *J. China Univ. Min. Technol.* **2018**, *47*, 969–978.
18. Guo, X.; Zhao, Z.; Gao, X.; Wu, X.; Ma, N. Analytical solutions for characteristic radii of circular roadway surrounding rock plastic zone and their application. *Int. J. Min. Sci. Technol.* **2019**, *29*, 263–272. [CrossRef]
19. Wang, W.; Guo, G.; Zhu, Y.; Yu, W. Malignant development process of plastic zone and control technology of high stress and soft rock roadway. *J. China Coal Soc.* **2015**, *40*, 2747–2754.
20. Guo, X.; Li, C.; Huo, T. Shapes and formation mechanism of the roadway plastic zone under partial confining pressure. *Geomech. Eng.* **2021**, *25*, 509–520.
21. Liu, H.; Guo, L.; Zhao, X. Expansionary Evolution Characteristics of Plastic Zone in Rock and Coal Mass Ahead of Excavation Face and the Mechanism of Coal and Gas Outburst. *Energies* **2020**, *13*, 984. [CrossRef]
22. Guo, X.; Guo, L.; Li, C.; Ma, N.; Zhao, Z.; Huo, T. A Quantitative Assessment Method of Roadway Rockburst Risk Based on the Plastic Zone Shape Coefficient. *J. China Univ. Min. Technol.* **2021**, *50*, 39–49.

23. Aker, E.; Kühn, D.; Vavryčuk, V.; Soldal, M.; Oye, V. Experimental investigation of acoustic emissions and their moment tensors in rock during failure. *Int. J. Rock Mech. Min. Sci.* **2014**, *70*, 286–295. [CrossRef]
24. Rong, H.; Wang, H.; Wang, Z.; Feng, M.; Mu, B.; Wang, Z. Experimental Research on Influence of Size Effect on Compression Mechanical Strength and Failure Characteristics of Rock. *Railw. Stand. Des.* **2017**, *61*, 96–100.
25. Li, D.; Liu, M.; Han, Z.; Zhou, Z. Dynamic compressive mechanical properties of bedding sandstone with pre-existing hole. *J. China Coal Soc.* **2019**, *44*, 1349–1358.
26. Yin, G.; Lu, J.; Zhang, D.; Li, M.; Deng, B.; Liu, C. Study on Plastic Zone and Permeability-increasing Radius of Borehole Surrounding Rock under True Triaxial Stress Conditions. *Rock Soil Mech.* **2019**, *40*, 1–10.
27. Yin, G.; Lu, J.; Li, X.; Liu, C.; Li, M.; Ma, B. Stability and Plastic Zone Characteristics of Surrounding Rock under True Triaxial Stress Conditions. *J. China Coal Soc.* **2018**, *43*, 2709–2717.
28. Zhou, Y.; Zhu, Q.; Li, D.; Ma, D. Experimental Study on Mechanical and Failure Characteristics of Sandstone with a Filled Elliptical Hole. *J. Railw. Sci. Eng.* **2019**, *16*, 9.
29. Li, C.; Li, X.; Li, D. Particle Flow Analysis of Fracture Characteristics of Marble with a Single Hole. *Chin. J. Eng.* **2017**, *39*, 1791–1801.
30. Wei, M.; Dai, F.; Liu, Y.; Li, A.; Yan, Z. Influences of Loading Method and Notch Type on Rock Fracture Toughness Measurements: From the Perspectives of T-Stress and Fracture Process Zone. *Rock Mech. Rock Eng.* **2021**, *54*, 4965–4986. [CrossRef]
31. Wei, M.; Dai, F.; Liu, Y.; Jiang, R. A fracture model for assessing tensile mode crack growth resistance of rocks. *J. Rock Mech. Geotech. Eng.* 2022; *in press*. [CrossRef]
32. Kang, H.; Yi, B.; Gao, F.; Lv, H. Database and Characteristics of Underground In-situ Stress Distribution in Chinese Coal Mines. *J. China Coal Soc.* **2019**, *44*, 23–33. [CrossRef]
33. Xia, S.; Lin, R.; Cui, X.; Shan, J. The application of orthogonal test method in the parameters optimization of PEMFC under steady working condition. *Int. J. Hydrog. Energy* **2016**, *41*, 11380–11390. [CrossRef]
34. Fan, D.; Chen, Y. *Probability Theory and Mathematical Statistics*; Zhejiang University Press: Hangzhou, China, 1996.
35. Oktem, H.; Erzurumlu, T.; Uzman, I. Application of Taguchi optimization technique in determining plastic injection molding process parameters for a thin-shell part. *Mater. Des.* **2007**, *28*, 1271–1278. [CrossRef]
36. Cui, W.; Li, X.; Zhou, S.; Weng, J. Investigation on process parameters of electrospinning system through orthogonal experimental design. *J. Appl. Polym. Sci.* **2007**, *103*, 3105–3112. [CrossRef]
37. Li, D.; Song, X.; Gong, C.; Pan, Z. Research on cementitious behavior and mechanism of pozzolanic cement with coal gangue. *Cem. Concr. Res.* **2006**, *36*, 1752–1759. [CrossRef]
38. Białek, J.; Wesołowski, M.; Mielimąka, R.; Sikora, P. Deformations of Mining Terrain Caused by the Partial Exploitation in the Aspect of Measurements and Numerical Modeling. *Sustainability* **2020**, *12*, 5072. [CrossRef]
39. Shi, X.; Zhang, J. Characteristics of Overburden Failure and Fracture Evolution in Shallow Buried Working Face with Large Mining Height. *Sustainability* **2021**, *13*, 13775. [CrossRef]
40. Zhang, G.; Zhang, Y. Partition failure characteristics of rock materal loading and unloading based on Mohr-Coulomb criterion. *J. China Coal Soc.* **2019**, *44*, 1049–1058.
41. Zhang, G.; Zhang, Y. Immediate roof first fracture characteristics of suberect and extremely thick coal. *J. China Coal Soc.* **2018**, *43*, 1220–1229.
42. Zhang, G.; Li, Q.; Xu, Z.; Zhang, Y. Roof Fractures of Near-Vertical and Extremely Thick Coal Seams in Horizontally Grouped Top-Coal Drawing Method Based on the Theory of a Thin Plate. *Sustainability* **2022**, *14*, 10285. [CrossRef]
43. Feng, P.; Zhao, J.C.; Dai, F.; Wei, M.D.; Liu, B. Mechanical behaviors of conjugate-flawed rocks subjected to coupled static-dynamic compression. *Acta Geotech.* **2022**, *17*, 1765–1784. [CrossRef]
44. Li, J.; Lian, X.Y.; Li, C.; Wu, Z.; Wang, J. Failure mechanism and support system of roofs in advance areas affected by mining under the condition of soft rock stratum. *Front. Earth Sci.* **2022**, *10*, 936029. [CrossRef]